AUTHOR(S): OKON, E., SHEHU, H. and GOBINA, E.

TITLE: Evaluation of the performance of α-alumina nano-porous ceramic composite membrane for esterification applications in petroleum refinery.

YEAR: 2018

Publisher citation: OKON, E., SHEHU, H. and GOBINA, E. 2018. Evaluation of the performance of α-alumina nano-porous ceramic composite membrane for esterification applications in petroleum refinery. Catalysis today [online], 310, pages 146-156. Available from: https://doi.org/10.1016/j.cattod.2017.05.089

OpenAIR citation: OKON, E., SHEHU, H. and GOBINA, E. 2017. Evaluation of the performance of α-alumina nano-porous ceramic composite membrane for esterification applications in petroleum refinery. Catalysis today, 310, pages 146-156. Held on OpenAIR [online]. Available from: https://openair.rgu.ac.uk

Evaluation of the Performance of α-alumina nano-porous ceramic composite membrane for Esterification applications in Petroleum Refinery.

Edidiong Okon, Habiba Shehu and Edward Gobina*.
Center for Process Integration and Membrane Technology (CPIMT), School of Engineering. The Robert Gordon University Aberdeen, AB10 7GJ, United Kingdom.
E-mail: e.p.okon@rgu.ac.uk, h.shehu@rgu.ac.uk *Corresponding Author: e.gobina@rgu.ac.uk. Phone No.: +44(0)1224262348.

Abstract

The carrier gas permeation performance through α-alumina nano-porous ceramic membrane was investigated in this study. The four carrier gases used for the study were argon (Ar), helium (He), nitrogen (N_2) and carbon dioxide (CO_2). The experiments was carried out at the gauge pressure drop of 0.10 – 1.00 bar at 80 ^oC. The α-alumina membrane was prepared using the sol-gel dip-coating techniques. The dip-coated membrane exhibited a higher molar flux with He (0.046mol $m^{-2}s^{-1}$) and Ar (0.037mol $m^{-2}s^{-1}$) with a much lower flux for N_2 (0.037mol $m^{-2}s^{-1}$) and CO_2 (0.035 mol $m^{-2}s^{-1}$) at 0.30 bar. The membrane recorded a huge decrease of permeance with the four carrier gases in the range of 9.81783E-07 mol m^{-2} s^{-1} Pa^{-1} to 1.23237E-06 mol m^{-2} s^{-1} Pa^{-1} at 0.50 bar. The gas flow rate increased with respect to the pressure drop across the membrane. A plot of the inverse square root of the gases molecular weight showed a linear dependence on the gas permeance. The order of the gas flow rate with respect to the mean pressure was He > Ar > CO_2 > N_2. The membrane was characterised using different methods including liquid nitrogen physisorption (Quantachrome instrument 2013) and scanning electron microscopy (Zeiss EVO LS10 SEM). The liquid nitrogen adsorption isotherm were described using the BET and BJH methods. The BET surface area of the 7th dip-coated membrane was found to be higher (5.991 m^2/g) in contrast to the 8th dipped (3.840 m^2/g). The BJH pore size distribution of the membrane show a reduction pore size after the modification process. The BET isotherms of the membrane indicated a type IV isotherm with hysteresis on the curve indicating that the membrane can undergo a capillary condensation in the mesoporous region. The SEM/EDAX of support showed a clear surface without evidence of crack while the SEM micrograph of the silica membrane exhibit a bonding on the surface membrane as result of the modification process.

Key words: Tubular membrane, characterisation, chromatogram, carrier gas transport, Knudsen mechanism, adsorption isotherm and esterification.

1. Introduction

Membrane separation has shown a lot of advantages such as high efficiency and energy saving in contrast to other conventional methods of separation such as absorption, adsorption and crystallisation. Due to these advantages,

membrane separation has been widely accepted in large-scale application during the last decades. Based on the materials, membranes may be classified into two different types: Organic membrane such as polymeric membranes and inorganic membranes such as ceramic membrane. Inorganic membranes possess some outstanding properties such as chemical stability, thermal stability, easy cleaning and non-swelling nature. Hence inorganic membranes are widely used in high-temperature separation processes and as membrane reactors [1]. Gas separation is an important aspect of operation that has attracted a lot of attention in the chemical industries. The separation of air into nitrogen and oxygen and the removal of the volatile organic compounds from effluent streams are examples of gas separation [2]. Recently, membrane-based gas separation has been the topic of the day because of its numerous advantage such as lower energy consumption, ease of operation, low operation and capital cost; compared to tradition method of gas separation. Membrane may be defined as an interphase between two bulk phases. Currently, membrane-based separation are being employed in a lot of applications including nanofiltration, reverse osmosis, ultrafiltration and microfiltration [2]. The use of membranes and membrane technologies for the selective removal of product to shift the equilibrium towards higher yield of the product in equilibrium limiting reaction systems have attracted a lot of attention [3],[4]. Generally, esterification reactions are usually limited by equilibrium and therefore do not attain completion [5],[3]. The major role of the membrane in esterification in reactions is that it can work both as a catalyst and also in the removal of the product by reacting with the reactants (carboxylic acid and alcohol) and the catalyst and shifting the equilibrium to the product side by selectively removing water from the bulk of the reaction [3]. Solvents are basic consumables in industries such as chemical, pharmaceutical, and agriculture. They are manufactured from petrochemical feedstock obtained from natural gas and crude oil [6]. Studies have shown that the use of some petrochemical solvents may result in serious health and environmental problems. One of the major challenges faced by the petrochemical industry has been the replacement of traditional petroleum-derived solvents [7]. It is therefore essential to develop new solvents with less toxic and hazardous characters [8]. Ethyl lactate (EL) is one of the solvents in high demand in the chemical and petroleum industry and it is a sustainable alternative organic solvent with advantages that include biodegradability, non-carcinogenic, non-corrosive and non-ozone depleting and is miscible with water and hydrocarbons. Because of its outstanding advantages, EL has been described by the U.S Environmental Protection Agency (EPA) as a ‘’green solvent’’ [9]. EL is therefore a suitable replacement for a number of hazardous organic solvents including toluene, benzene, chloroform, xylene and hexane in the petroleum industry. It is used in different industries such as food, pharmaceutical, paint, adhesive, agriculture and petroleum refinery [10].

The combination of membrane separation process with chemical reaction process have attracted a lot of attention due to their high selectivity [11],[12]. In recent years, silica membranes have been widely investigated for use in gas separations [13]. Silica membranes are normally in the form of a silica layers placed on a ceramic support such as alumina and the deposition is usually carried out by the sol-gel or chemical vapour deposition (CVD) of silica precursors [14]. Generally, the sol-gel process has been widely used for the modification of alumina and silica-based inorganic membranes [2]. Dip-coating is a convenient membrane preparation method which has been widely used to produce ceramic membranes to microporous layers from porous supports [15]. In the dip–coating techniques, a wet layer of ceramic particle is deposited on a porous support by coating the surface of the dry support with a particle-dispersed suspension or a suitable sol such as colloidal boehmite, followed by drying and thermal treatment of the support [15],[2]. According to Zhu et al. 2011 [15], the conventional dip-coating method involves two steps: support dipping and support withdrawal. However, the dip-coating parameters such as dipping speed, viscosity of the sol, immersion and drying time affect both the thickness and the pore size distribution of the membrane [16]. In the support dipping step, the effect of capillary-filtration dominates, particles are deposited and accumulated on the surface of the support because of the suction of the solvent into the pores of the support under the capillary force. Though a lot of particles gets deposited on the pinhole defect area based on the self-repairing mechanism, the process of the deposition of particles because of the capillary-filtration cannot be controlled and hence needs more repetitions. Similarly, in the case of the support withdrawal, this step is dominated by the film-coating, an adhering particle layer is formed by the drag force applied by the support during withdrawal from suspension [15].

The transport of gases through porous membranes can be explained using various transport mechanisms based on several factors such as the size of the permeating gas molecules, the membrane material, the driving force (pressure and temperature) and the average pore size [17],[18]. The different mechanisms of gas transport through porous membranes include surface diffusion, Knudsen diffusion, capillary condensation, viscous flow, and molecular sieving mechanisms [19],[20]. Knudsen mechanism occur when the mean free path of the gas molecule is greater than the pore size. In such case, collision of the gas molecule with the pore wall are more frequent than the collision between molecules. Viscous flow mechanism takes place if the mean free path of the gas molecule is smaller than the pore size and diffusion of gases and takes place basically through molecule-molecule interaction than molecule to pore wall. Surface diffusion takes place when the permeating gas molecule exhibit a strong affinity for the membrane surface and adsorb along the pore walls. Capillary condensation occur when the pores are completely filled with the condensed gas at certain critical relative pressures mostly in mesopores and

macropores [21]. Gas separation by molecular sieving mechanism takes place when the pore diameter of the inorganic ceramic membrane are roughly the same as those of the permeating gas molecules [22].

Synthesized membranes can be characterised using various methods. Scanning electron microscopy is normally used in order to examine the surface morphology and the x-section of the membrane. Liquid nitrogen physisorption analysis is used to determine the pore structure of the membrane. According to IUPAC (International Union of Pure and Applied Chemistry), the physisorption isotherm can be classified into six different types [23]; Type 1 isotherm is characterised by the adsorption in the non-porous microporous region at a low relative pressure. Type ll is characteristic of non-porous or macroporous adsorbents with the formation of a multilayer of adsorbate (gas molecule) on the surface of the adsorbent. Type III is characteristic of a non-porous or macroporous layer with weak interaction between the gas molecule and the membrane material. Type IV isotherm reflects a macroporous material which involves the coverage of the monolayer–multilayer on the external surface which is followed by capillary condensation in the mesoporous region with the formation of hysteresis loop based on the shape of the pores. Type V isotherm is characteristic of a mesoporous material and involves the weak interaction between the permeating gas molecule and the membrane material. Type V1 isotherm takes place in a highly uniform surface [23],[16]. Fourier transform infrared spectroscopy (FTIR) is one of the most useful techniques for the characterisation of the membrane surface [24]. Jin et al. 2011 [15] prepared an α-Al_2O_3 microfiltration pinhole-free membrane using a modified dip-coated process to prevent pinhole defects in ceramic membranes. In their results, they found that pinholes in membrane could be effectively avoided by applying a suspension flow velocity of 50 mms^{-1} and a withdrawal speed of 4 mms^{-1} via a single coating-sintering procedure. McCool et al. 2003 [13], used the dip-coating method for the membrane fabrication and deposition on a polished surface of an alumina support disk and reported the gas permeation for N_2, Ar, O_2 and He gas to be strongly governed by Knudsen mechanism. Xomeritakis et al 2003 [25] perform an experiment on organic-templated silica membranes. Gas and vapour transport properties. In their results, they found that the silica coated membrane exhibited permeance values as high as 10^{-7} to 10^{-6} $molm^{-2}s^{-1}Pa^{-1}$.

Although a lot of work has focused on the production of this solvent by the esterification process, no previous work has considered testing the carrier gas with the membrane to check the compatibility of the carrier gas with the GC before being utilised for the analysis of the esterification product. This work incorporates the analysis of the carrier has with the membrane to see the permeation rate of the gases with the membrane before employing this gas as a carrier gas for the analysis of esterification product. The membrane was prepared using the sol-gel

dip-coating method. The result was determined by plotting the flow rate against the gauge pressure and the flux of the gases against the pressure drop across the membrane.

2. Experimental Design and Procedure

2.1 Support

A 15 nm pore size commercially available tubular ceramic support, consisting of 77% Al_2O_3 and 23% TiO_2 with the porosity of 45% was used for the study. The support possesses an inner and outer diameter of 7 and 10mm respectively with a permeable length of 34.2mm and a total length of 36.6mm. The support was supplied by ceramiques techniques et industrielles (CTI SA), France.

2.2 Preparation of α-alumina nano-porous composite membrane

The membrane was prepared using the sol gel dip-coating process. The membrane preparation was carried out based on a patented method by Gobina 2006 [26]. The silica solution used for the membrane dip-coated consist of silicone elastomer, isopentane (2-methyl butane) and the curing agent. Prior to the preparation, the support was weighed to determine the actual weight before and after modification. 545 mL of isopentane (Sigma Aldrich ≥ 99%) was measured into 1000 mL glass measuring cylinder and 50 mL of silicon elastomer (Sigma Aldrich ≥ 99%) was added to the solution together with 5 mL of the curing agent (Sigma Aldrich ≥ 99%) which help in the polymer cross-linking process. The mixture was allowed to stir for 30 minutes on an electric stirrer to obtain homogeneity of the solution. Prior to the dipping of the support into the silica solution, both ends of the membrane support was carefully sealed to prevent the coating of inside surface of the support. The support was then dipped into the silica solution and allowed in the solution for 30 minutes. After 30 minutes, the support was carefully withdrawn from the solution and dried using a customised rotatory evaporator for 30 minutes at room temperature to allow the coating to adsorb on the membrane surface before it was transferred to the oven and dried for 2 hrs at a constant temperature of 65 ^oC [27]. Table 1 shows the composition of the silica solution that was used for the experiment. Figure 1 describe the schematic membrane dip-coating set-up.

Table 1: Composition of the Silica Compound

Components	Quantity (mL/g)
Iso-pentane (2-methylbutane)	545mL
Sylgard®184 Silicone Elastomer	50mL
Sylgard®184 Curing agent	5mL
Measuring cylinder	1000mL
Weight of membrane before modification	48.3g

Weight of membrane after modification	49.1g

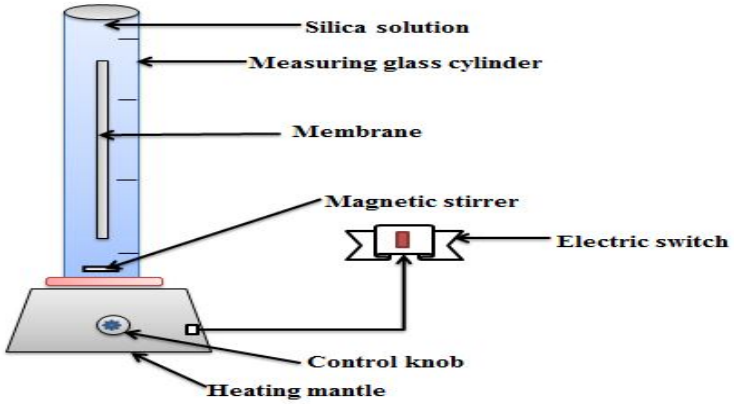

Figure 1: Schematic diagram of the dip-coating membrane setup.

2.3 The permeation cell

The permeation cell consisted of a stainless steel tube with membrane centralized in the tube using graphite seals at either ends. Through the use of various connections fittings and values the cell permits the measurement of the gas flux through the membrane at various feed pressures. A heating tape was wrapped over the stainless steel which enables high-temperature studies to be carried out. Prior to permeation experiments, a leak test was carried out by monitoring the downstream pressure while the system remained totally closed and pressurized [27].

2.4 Carrier Gas Transport Through α-alumina nano-porous Membrane

The transport of the single gases with α-alumina nano-porous ceramic membrane was carried out using four different gases which could serve as carrier gases for esterification reaction including argon (Ar), helium (He), carbon dioxide (CO_2) and nitrogen (N_2) with the purity of at least 99.999 (% v/v). The carrier gases were supplied by BOC, UK. The permeability experiment was carried out at the gauge pressure of between 0.10 -1.00 bar and temperature range of 25 -100 ^oC. The different carrier gases were feed into the reactor through the feed gas opening where the gases interact with the membrane and exit through the permeate. The flow rate of the gases was obtained using a flow meter by varying gauge pressure. Fig. 2 shows the carrier gas permeation setup. The tested carrier gases were further coupled with gas chromatograph (GC) in the analysis of esterification reaction product.

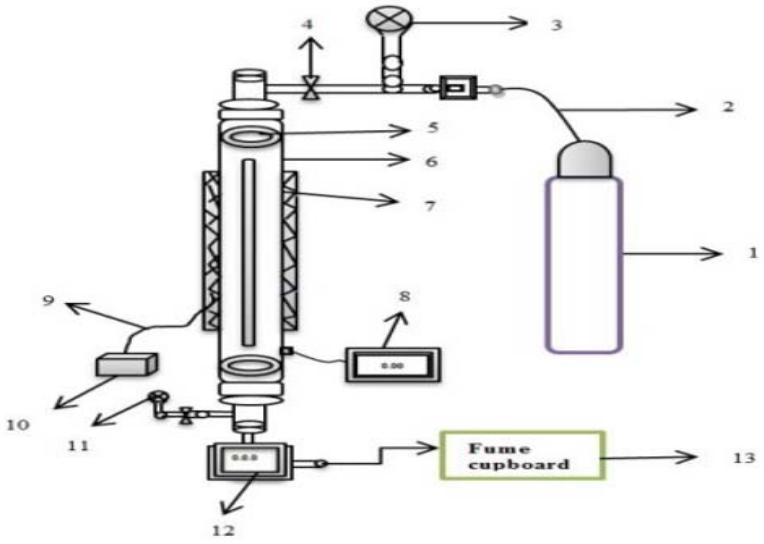

Figure 2: Carrier gas permeation test setup which consists of **; carrier gas cylinder (1), gas feed inlet (2), permeate pressure gauge (3), control valve (4), O-ring graphite seal (5), reactor (6), heating tape (7), temperature regulator (8), thermocouple (9), thermocouple box (10), retentate pressure gauge (11), flow meter (12) and fume cupboard (13).**

2.5 GC-MS Analysis of Esterification Product using Helium as carrier gas

2.5.1 Batch Process Esterification reaction

Lactic acid (99.9 wt %) and ethanol (99.9 wt %) used for the batch process esterification were all purchased from Sigma-Aldrich, UK and were used as received without further purification. The catalyst used in the experiments was amberlyst 36 commercial solid cation exchange resin also purchased from Sigma-Aldrich, UK. Helium gas (99.98 % purity) was used as carrier gas and was obtained from BOC, UK. The deionised water used for the washing of the catalysts was supplied by the Centre for Process Integration and Membrane Technology (CIPMT), Robert Gordon University (RGU), Aberdeen, UK. A 500 mL batch reactor, reflux condenser and the vacuum pump used for the esterification process were all purchased from Sigma Aldrich, UK.

Prior to the analysis, 5g of the fresh commercial cation exchange resin was placed 0in a 50 mL beaker and was rinsed with 2 mL of deionised water and 10 mL of ethanol and oven dried at 65 ^{o}C for 24 hrs to remove poisonous substances and moisture completely. A similar method to that of Zhang et al. [28] was adopted. After the catalyst cleaning process, 30 mL of lactic acid with 5g of the amberlyst 36 cation-exchange resin was charged into the reactor and heated to 100 ^{o}C. After the desired temperature was attained, 50 mL of ethanol (which had been previously heated separately) was added to the mixture in the reactor. The stirring and heating of the reaction

mixture was achieved using a magnetic hot plate with a stirrer. The stirrer speed was controlled at the speed of about 400–800 rpm [29]. Table 2 shows the composition of the solution and the weight of the cation-exchange resin that was used for the experiment.

Table 2: Composition of solvents used for the esterification reaction.

Components	Quantity (mL/g)
Lactic acid	545mL
Amount of Ethanol for esterification	50mL
Amount of Ethanol for catalyst cleaning	10mL
Deionised water	2mL
Beaker	50mL
Weight of amberlyst 36	5g
Batch reactor	500mL

2.5.2 GC-MS Analysis

After the esterification process, about 1 mL of the reactant mixture was taken out for analysis with the GC-MS analysis using helium gas (99.98% purity) as the carrier gas. An Agilent technologies 7890B autosampler Gas Chromatograph (GC) system coupled with Agilent technologies 5977A mass spectrometry detector (MSD) was used to determine the concentration of the products which were subsequently used to determine the kinetics of the esterification reaction. A microliter syringe (Hamilton HM80300 microliter (TM) syringe) was used for sample preparation before it was inserted into the GC vial for injection. Fig. 3 shows the GC-MS instrument that was used for the esterification analysis [29].

Figure 3: Agilent technologies 7890B autosampler Gas chromatography (GC) system coupled with Agilent technologies 5977A mass spectrometry detector (MSD) at the Centre for Process Integration and Membrane Technology (CPIMT), RGU.

As part of the quality control measures, a blank analysis was carried out in order to clean the GC column prior to the sample analysis. Ar and N_2 gas were used as the detector gases. A capillary column with the column dimensions of 30 m x 250 µm x 0.25 µm was used for the analysis and at the heating rate of 10 ^oC/min, at 63.063 kPa. The Helium gas temperature was set at 40 ^oC with the flow rate of 1.2 mL/min and equilibration time of 0.25 mins while the inlet pressure was 100 PSI. The oven temperature was programed at 40 ^oC with the holding time of 2 mins at maximum operating temperature of 25 ^oC. The sample scanning rate was 9.773 mins. The solvent analysis was set on split mode with the split ratio of 50:1. The sample vial was carefully cleaned prior to each analysis. The sample was carefully inserted into the sample rage embedded in the injector port of the GC-MS where the carrier gas transfers the solvent to the GC column. The Agilent Technologies NIST Mass hunter software program was used for data collection. Both quantitative and qualitative analysis of the reaction product in the presence of each cation-exchange resin at 100 ^oC were performed in triplet and the chromatogram, mass spectra, retention time and peak area were compared with that of the commercial ethyl lactate solvent [29].

2.6 Membrane characterisation

The membrane was characterised using different analytical methods including liquid nitrogen adsorption/desorption method at 77K. The Liquid nitrogen automated gas sorption analyser (Quantachrome

instrument version 3.0) was used to determine the pore size distribution and the total surface area of the membrane. The isotherms were described using the Brunauer Emmett and Teller (BET) and the Barrett-Joyner-Halenda (BJH) methods. The surface morphology of the membrane was carried using the Zeiss EVO LS10 scanning electron microscopy coupled with the energy dispersive x-ray analyser (SEM/EDAX) to determine the thin layer on the coated surface of the membrane. Fourier transform infrared coupled with attenuated total reflection (Nicolet iS10 FTIR-ATR) was used for the structural analysis of both the support and silica membranes. Permeation measurement were also applied to determine the gas flow rate.

2.7 Equations for Permeation Rate Calculations

The surface area of the membrane was calculated using the formula [30]:

$$\mathbf{A} = \frac{\mathbf{\pi L(r_1 - r_2)}}{\mathbf{\ln(r_1 / r_2)}} \quad \text{.....(1)}$$

Where A = membrane surface area (m^2), L = length of the membrane (m), r_1 = outer pore radius (m), r_2 = inner pore radius (m), π = constant (3.142) [30].

The gas flux was calculated using the following equation:

$$J = \frac{Q}{A} \quad \text{.....(2)}$$

Where J = flux (mol m^{-2} s^{-1}), Q = flow rate of the gases (mol s^{-1}), A= membrane surface area (m^2). The gas permeance was obtained using the following equation [31]:

$$\overline{P} = \frac{J}{\Delta P} \quad \text{.....(3)}$$

Where ΔP is the pressure drop across the membrane (bar), J = flux (mol $m^{-2}s^{-1}$), P is the peremance (mol m^{-2} s^{-1} Pa^{-1}) [31].

3. Result and Discussion

3.1 FTIR of Support and Silica Membrane

Figure 4 present the FTIR of the support (3a) and that of silica membrane (3b) after the dip-coating process. From figures 4a and b, comparing the FTIR of the support and that of the silica membrane, it can be seen that the support membrane exhibited 3 bands on the spectra while the silica coated membrane exhibited upto 5 bands on the spectra. From Fig. 4a, it was found that the band at 2335.00 indicated the C-H functional group while the band at 2167.34 and 1977.73 showed the presence of C=O and functional group. It was suggested that the C=O functional

groups indicate that these could be due to the alumina oxide in the original support. From Fig 4b, it was found that the band at 2356.07 indicated the C-H functional group while the bands at 2165.58 and 1257.44 were attributed to the stretching vibration of C=O and C-O functional groups respectively. Also the bands at 1088.10 and 1011.89 depicts C-O functional group. It was suggested that the C=O and C-O functional groups on the silica membrane spectra could originate from the silica solution that was used for the membrane preparation process.

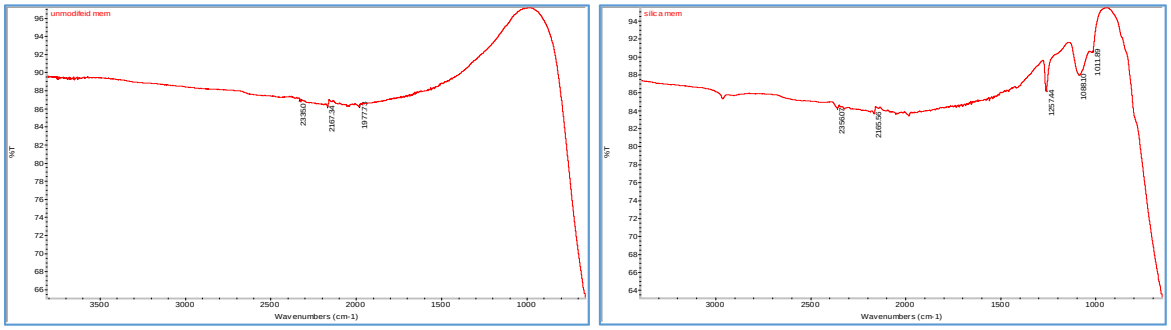

(a) (b)

Figure. 4a and b: FTIR for unmodified support membrane (3a) and FTIR for silica coated membrane (3b).

3.2 Gas permeation results

Figure 5 depicts the relationship between the permeance as a function of the feed gauge pressure for the four gases between the gauge pressure range of 0.10 – 1.00 bar and at 80 ^{o}C. From the result obtained in figure 5, it can be seen that the gas permeance decrease with an increase in gauge pressure across the membrane [32]. It can also be seen that He gas with the least molecular weight exhibited a huge decrease in contrast to other gases. Between the gauge pressures of 0.10 - 0.20 bar, all the gases exhibited a sharp decrease. This sharp decrease was attributed to the mass transfer limitation. It was also observed that Ar and CO_2 gases with a higher molecular weight exhibited the least permeance. This confirms a statement by Wall et al. 2010 [33] that the gas transport through the membrane is dependent on the molecular weight of the gases as the gases permeate through the pores of the membrane. The order of the gas permeance with respect to the feed gauge pressure was found to be He > Ar > N_2 > CO_2. This confirms the fact that Helium gas might be a suitable carrier gas for the analysis of the esterification reaction product for applications in petroleum refinery.

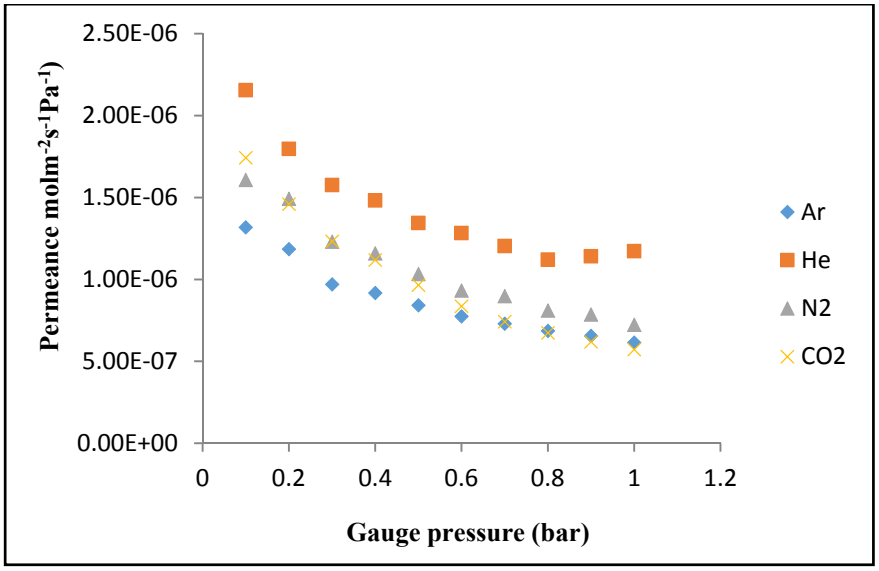

Figure 5: Permeance ($molm^{-2}s^{-1}Pa^{-1}$) against feed gauge pressure (bar) at 80 °C.

According to Araki et al. (2007) [34], the linear proportionality of gas permeance on the inverse square root of the gas molecular weight indicate the fact that the gas transport through silica membrane is as the result of Knudsen mechanism of transport. Figure 6 present the relation between the gas permeance and the inverse square root of the gas molecular weight at 0.30 bar and at 80 °C. From the results obtained in figure 6, it was found that Ar, N_2 and CO_2 gases showed a linear proportionality of permeance indicating Knudsen flow mechanism of transport except for He gas. This was in accordance with a similar result by McCool et al. [13] where the gases exhibited a linear proportionality of permeance as described by Knudsen mechanism of gas transport. It was suggested that there could be another mechanism of transport that was in operation for He gas at 0.30 bar and 80 °C.

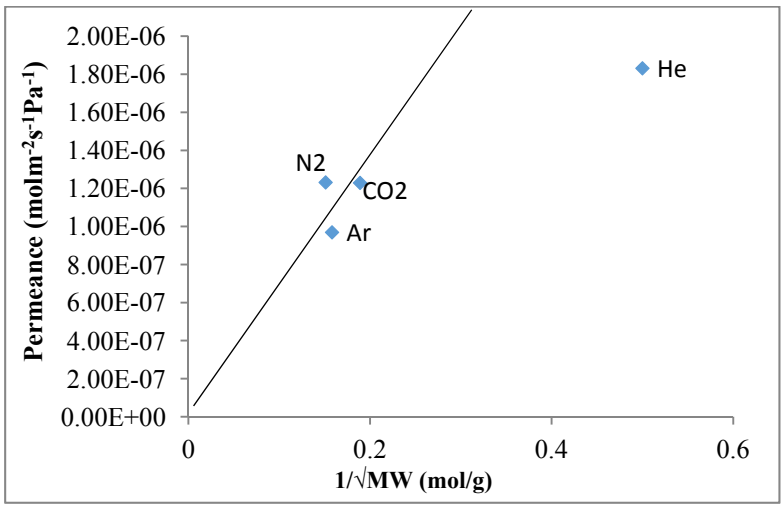

Figure 6: Gas permeance ($molm^{-2}s^{-1}Pa^{-1}$) against the inverse square root of molecular weight (g/mol).

Figure 7 depicts the relationship between the permeance and the inverse viscosity of the gases at the gauge pressure range of 0.10 – 1.00 bar and at 80 °C. From the result obtained in figure 7, it can be seen that the Ar and N_2 gases with the viscosity values of 22.9 and 17.81 Pas^{-1} exhibited a lower permeance in contrast to He and CO_2 gases with the viscosity value of 20.0 and 15.0 Pas^{-1} respectively. For a gas flow to be represented by the viscous flow mechanism, the gases with the higher viscosity value must show a lower permeance. From the result obtained, it was suggested that the gas flow was based on the viscous flow mechanism of gases transport. It was also observed that Ar and N_2 gases also pass through the linear line while He and CO_2 deviated from the trend. The order of the gas viscosity with respect to the gas permeance was given as He > N_2 > CO_2 > Ar.

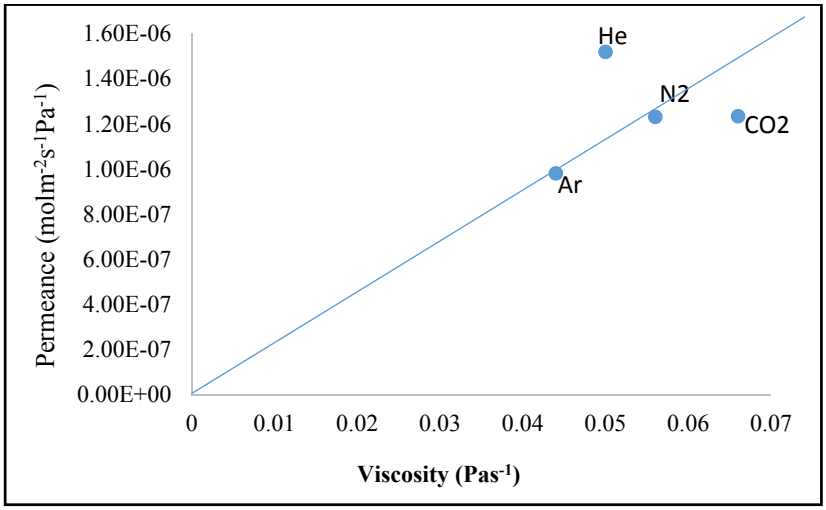

Figure 7: Gas permeance ($molm^{-2}s^{-1}Pa^{-1}$) against the inverse viscosity (Pas^{-1}).

Figure 8 depicts the relationship between the gas flow rate and the mean gauge pressure at 80 °C. From the result obtained in figure 8, it can be seen that the flow rate of the gases increases linearly with respect to the feed gauge pressure at 80 °C, suggesting that the membrane was defect-free due to the interaction with gases. According to McCool et al. [13], the flow rate of the gases depend on the molecular weight of the gases. From the result obtained in figure 8, it can be seen that He gas with the least molecular weight exhibited a higher flow rate followed by Ar gas. Although the permeation of the gases was not based on their respective molecular weight, the gas flow through the membrane could have been as a result of the Knudsen flow mechanism of gas transport with the contribution of other mechanism. The sequential order of the gas flow rate with respect to the mean gauge pressure was given as He > Ar > CO_2 > N_2. From the result obtained from the permeation rate of the gases with the membrane, He and Ar gases were selected as the suitable carrier gases that could be employ for the analysis of the esterification reaction product when coupled with gas chromatography mass spectrometry. The experimental

error determine for the analysis of the flow rate with respect to the mean pressure showed a better correlation of the graph.

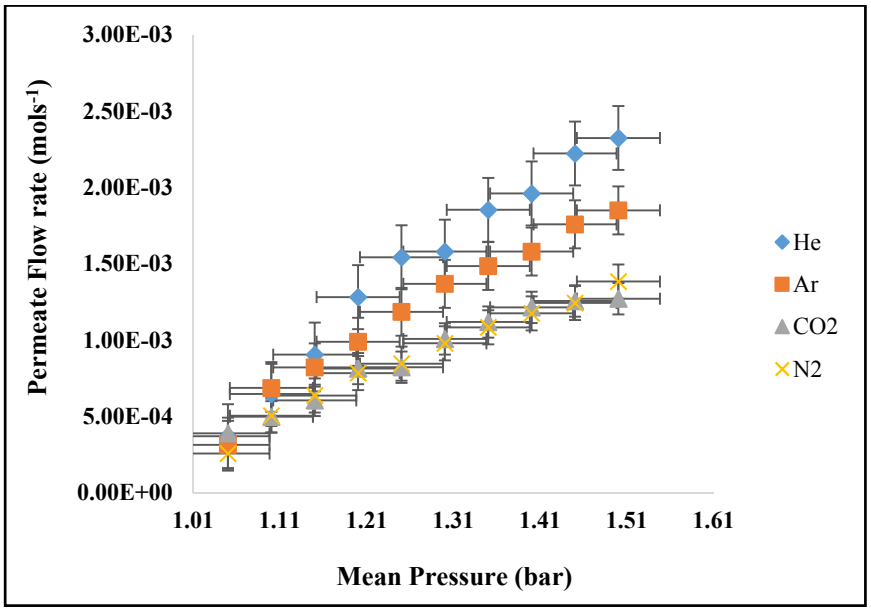

Figure 8: Gas flow rate ($mols^{-1}$) against the mean pressure (bar).

Figure 9 shows the gas flux ($mols^{-2}s^{-1}$) with respect to the gauge pressure (bar) at 80 ^{o}C. From the result obtained in figure 9, it can be seen that the flux of the gases increase linearly with respect to the gauge pressure. It was found that the helium gas with the least molecular weight showed a higher permeation rate followed by N_2 gas. Generally it can be seen that the gas flux followed their respective order of their molecular weight indicating that the gas permeation was in accordance with Knudsen mechanism. A similar results was obtained by Walls et al. 2010 [33]. The order of the gas flux with respect to the feed gauge pressure is given as $He > N_2 > Ar > CO_2$. It was found that Helium gas with the least molecular weight recorded the higher flux in contract to other gases. It was also observed that He and N_2 gas exhibited a higher correlation values of 0.9798 and 0.9537 in contrast CO_2 and Ar gas with R^2 value of 0.8587. Although CO_2 and Ar gas differs in molecular weight, the two gases were found to exhibit the same R^2 values indicating that the permeation of the two gases occur at the same rate.

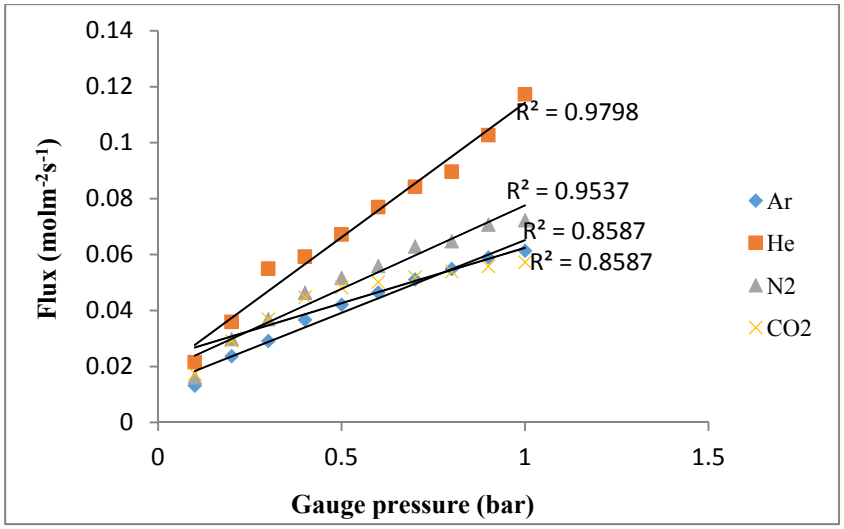

Fig. 9: Flux of the Ar (9a), N_2 (9b), He (9c) and CO_2 (9d) carrier gases at the gauge pressure range of 0.30 bar and 80°C.

Figure 10a-d depicts the relationship between the effect of temperature against permeance (In P) of the Ar (Fig.10a), He (Fig. 10b), N_2 (Fig. 10c) and CO_2 (Fig. 10d) gases between the temperature range of 333-393 K and at 0.30 bar for dip-coated membrane. From the temperature plot for the various gases, the activation energy for the transport of the gases were also calculated using equation 4 for comparison. Activation energy is an indicator of the barrier for the gases to permeate through the pores of the membrane and this implies that a lower value of the activation energy indicates a lower resistance for the gas transport through the membranes [35]. From the result obtained and tabulated in Table 3, it can be seen that Ar, He, CO_2 and N_2 gases exhibited a negative values of activation energy suggesting that there was effect of surface diffusion in operation as the gases penetrates through the pores of the silica membrane. Also, from the result obtained in figure 10a-d, it was observed that the calculated activation energy for the four gases were found to be different based on their adsorption capacities [22]. However, there was a positive activation energy for N_2 gas suggesting that this may be due to the effect of the heat of adsorption. It was also found that Ar (R^2 = 0.9987) and N_2 (R^2 = 0.9918) gases recorded a good linear regression fits suggesting that the gas transport occurred due to Knudsen diffusion in contrast to He (R^2 = 0.9300) and CO_2 (R^2 = 0.9557) gases.

$$P = P_O \exp\left(\frac{-E_a}{RT}\right) \quad \text{.....(4)}$$

Where P = permeance (mol $m^{-2}s^{-1}Pa^{-1}$), P_O = Arrhenius-type pre–exponential constant (m^2s^{-1}), T= temperature (K), Ea = activation energy ($Jmol^{-1}$) of surface diffusion or heat of adsorption and R= gas molar constant (8.314621 $Jmol^{-1}K^{-1}$).

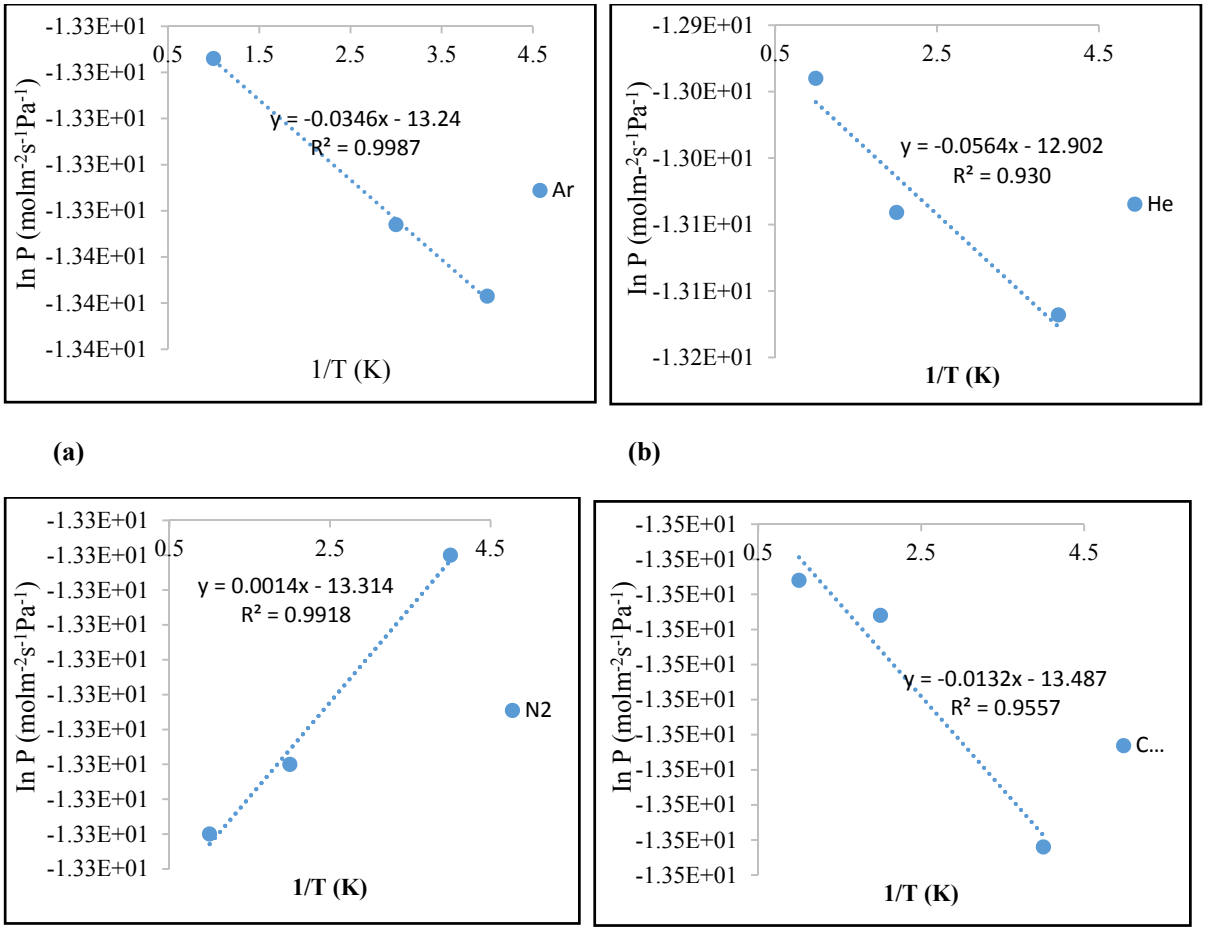

Fig.10a-d: Effect of temperature on the gas permeance of Ar (a), He (b), N_2 (c) and CO_2 (d).

Table 3: Calculated Activation Energy values for the gases with the dip-coated membrane at 0.40 bar between the temperature ranges of 333 – 393 K.

Gases	Activation energy value for Support	Activation energy value for Silica membrane
He	-4.689x10-4	-6.60x10^{-8}
Ar	-2.876x10-4	-2.49x10-8
N_2	0.116x10-4	-1.66x10-8
CO_2	-1.097x10-4	-7.48x10-9

3.3 GC-MS Results for Ester Product

Figure 11a shows the mass spectra of the esterification product catalysed by amberlyst 36 at 100 ^{o}C. From Figure 11a, it was found that ion number 45 with the highest peak reflected the structure of the ethyl lactate compound which was in accordance with that of commercial ethyl lactate compound from the NIST of the GC-MS. Although

the peak at ion 45 identifies that of the ethyl lactate, other ions in the spectra were represented by their respective compounds including methyl methanethiosulphonate (43), 2,4-pentanediol (44), methylazoxymthanol acetate (46), hydroxylamine, o-methyl (53), acetaldehyde, methoxy (56), methylal (58), acetoin (61), formic acid (71), 2,3-butandiol (73), oxirane (75), propane 2-fluoro (76), 2-butanediol (89) and ethanol,2-methoxy (91). This ions were suggested to arise as a result of some impurities in the ester product as the cation-exchange resin interact with the reactant solvent during the esterification process.

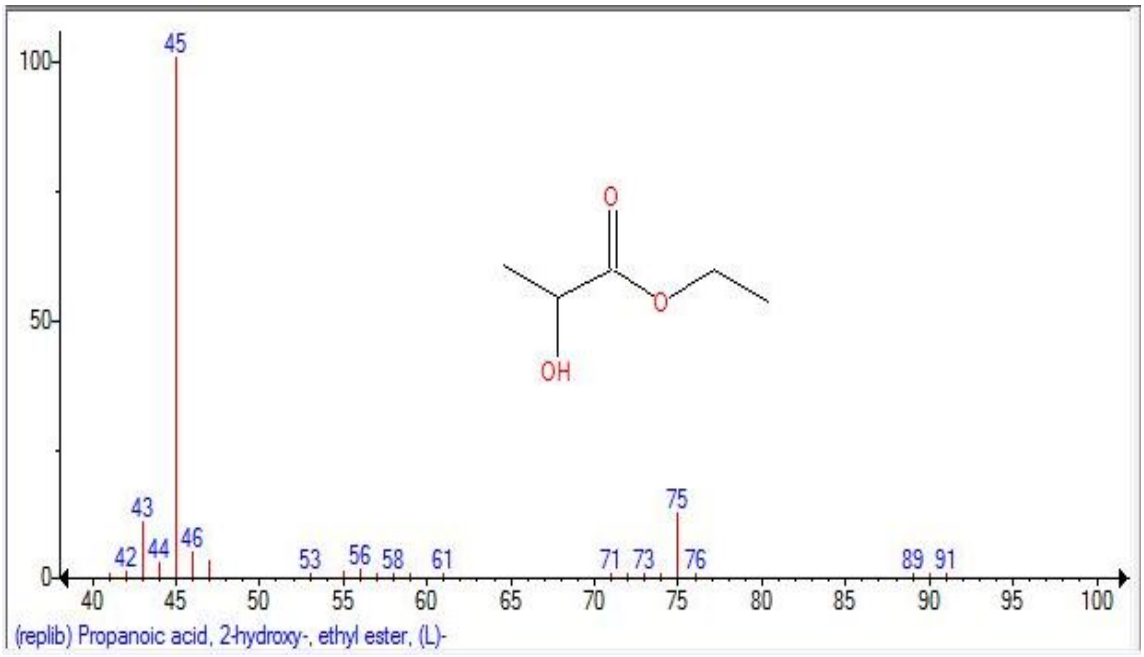

Figure 11a: Mass Spectra of the esterification product catalysed by amberlyst 36 at 100 ^{o}C.

Fig 11b shows the relationship between the mass abundance and retention time (min) of the esterification product catalysed by amberlyst 36. From the result of the chromatogram in figure 11b, it was found that the retention time of ethyl lactate for the resin catalyst increases with respect to their peak area. The first peak was found to elute at 2.128 minutes with the peak area of 131342329 m^2 while the last elution time was at 7.756 minutes having the peak area of 71378013 m^2. It was suggested that faster elution of peaks in the reaction product was due to the presence of the cation-exchange resin which also confirm that the produced esterification reaction product can be used for industrial purposes. From the obtained chromatogram results, helium gas was confirmed to be the suitable carried gas when coupled with gas chromatograph-mass spectrometry for the analysis of esterification product such as ethyl lactate which is a useful solvent in the petroleum industry, and this gas is strongly recommended to the industry for testing esterification product with GC-MS. Similar experiments are planned for the other cation exchange resins including amberlyst 16, dowex 50W8x and amberlyst 15 at the same temperature for comparison.

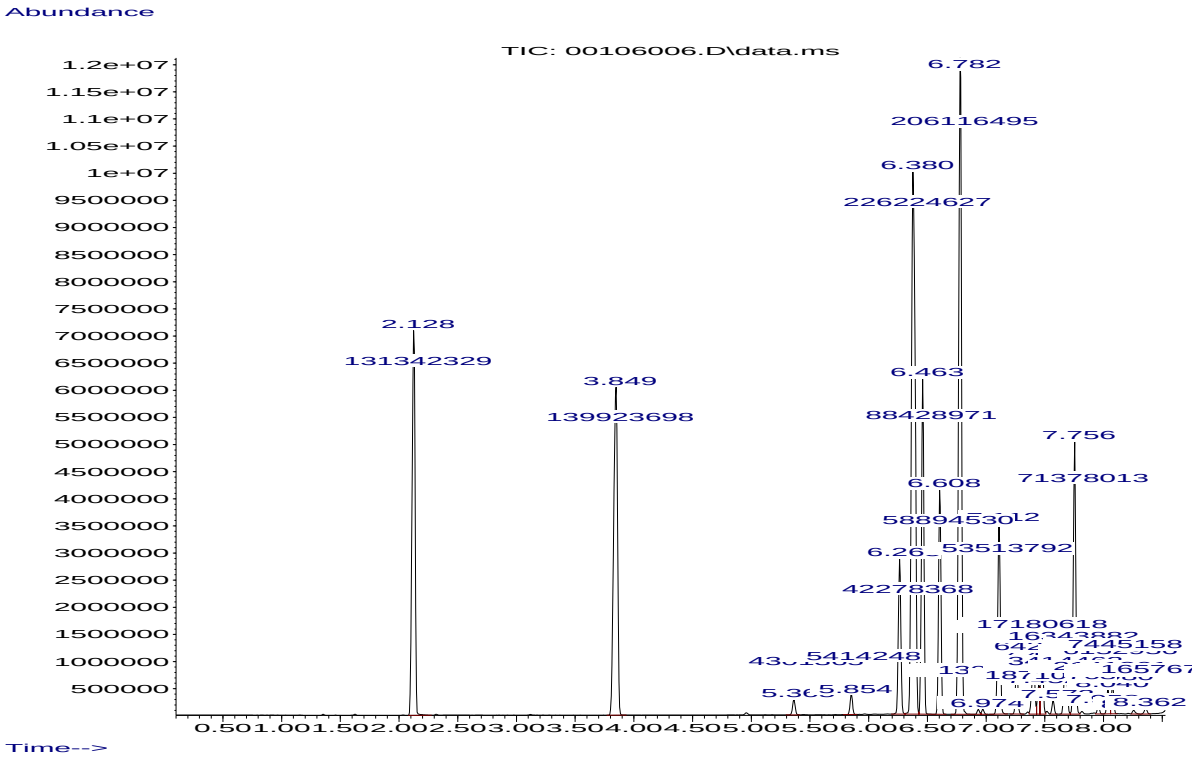

Figure 11b: Ion chromatogram for esterification product catalysed by amberlyst 36 at 100 ^{o}C

3.4 Liquid Nitrogen Adsorption/Desorption

Figure 12a and b depicts the BET surface area whereas figure 13a and b shows the BJH pore size of the 7th and 8th dip-coated membrane that were used for the study. The BET of the two membranes were studied for the purpose of comparison. From the result obtained in figures 12a and b, it was found that dip-coated membrane membranes possess hysteresis on their curves. The hysteresis in the both membranes suggest that the membrane can undergo a capillary condensation in the mesoporous region. It can be seen from figure 12a that the hysteresis of the 7th dip-coated membrane was more obvious in contrast to that of the 8th dip-coated membrane in figure 12b. From the results of the analysis obtained in figure 13a and b, it was found that both the 7th and the 8th dip-coated membranes possess a type IV and V isotherm which was in accordance with the mesoporous classification of the membranes. As expected, the surface area of the membrane was supposed to increase after each modification with a reduction in the pore size. From the result obtained in Table 4, it can be seen that the pore size of the membrane after the 8th dip was in accordance with the mesoporous classification of the membrane. From the results obtained, the surface area of the 7th dip-coated membrane was found to be higher than that of the 8th dipped membrane which also signifies the effect of the silica that was used in coating the surface of the membrane sample. The pore size of the silica membrane was analysed using the BJH method of the liquid nitrogen adsorption. From the result

obtained in figure 13a and b for the 7th and 8th dip respectively, the pore size of the 7th dip was found to be 3.713 nm while that of the 8th dip-coated membrane was 3.136 nm. As expected, it can be seen that there was a reduction in the pore size of the membrane after the silica modification process [36] which further confirms that the membrane was a mesoporous silica membrane.

Table 4: BET and BJH desorption summary for 7th and 8th dip-coated membranes

Sample	BET Surface area	BJH Pore size	Pore volume
7th dip-coated silica membrane	3.840m^2/g	3.713nm	0.001
8th dip-coated silica membrane	5.991m^2/g	3.136nm	0.018

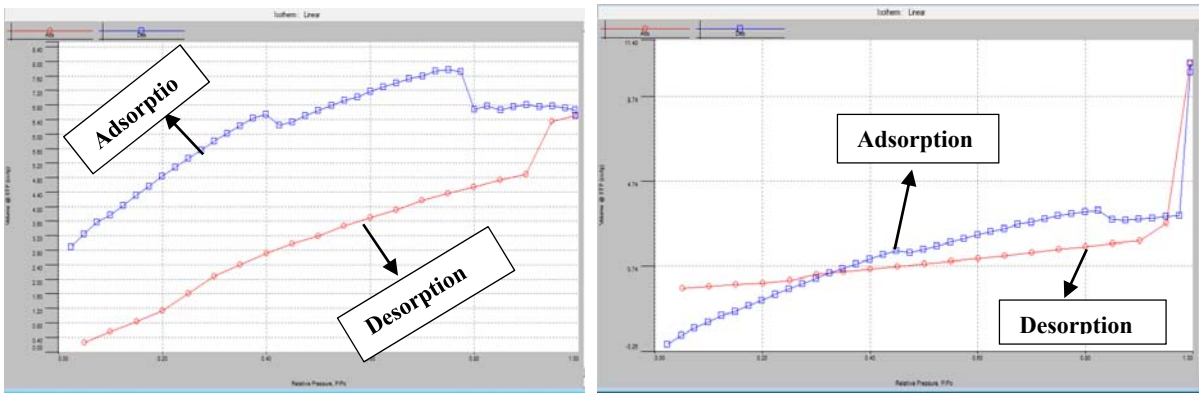

Fig. 12a and b: BET surface area of 7th dip-coated silica membrane (12a) and BET surface area of 8th dip-coated silica membrane (12b).

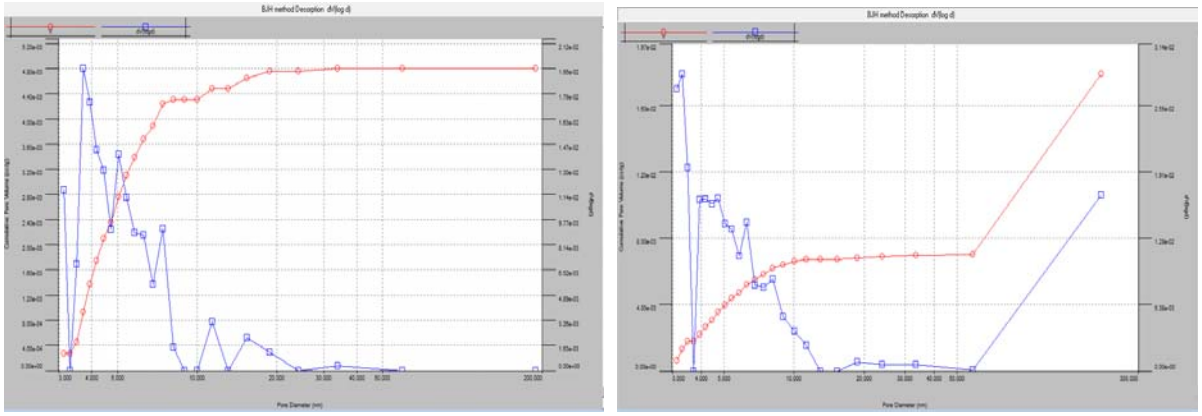

Fig. 13a and b: BJH pore size of 7th dip-coated silica membrane (13a) and BJH pore size of 8th dip-coated silica membrane (13b).

3.5 SEM/EDAX of the Support and Silica membrane

The scanning electron microscopy (SEM) micrographs and energy diffraction analysis of x-ray (EDAX) were carried out using a Zeiss EVO LS10 electron microscope. The surface morphology of the support and the silica membranes were further examined for the purpose of comparison. The SEM surface images of both the support and silica coated membrane are presented in figure 14a and b respectively. Figure 14 depict the EDAX of the membrane. The membranes were examine at the magnifications of 100 X and 400 X magnifications with the scale of 100 μm and 10 μm for the support and the silica mnembrane respectively. It was found that the fresh alumina support was made of different elemental composition including of Al_2O_3 and TiO_2. However, it suggested that SiO_2 was added to the other compounds already present in the membrane after the dip-coating process as shown on the EDAX spectra in figure 14. From the result obtained in figure 14a, it can be seen that the support exhibted a plain and clear surface without any evidence of carck on the surface indicating that the membrane was defect-free as confirmed by the permeation analysis. However, from figure 14b, it was observed that there was a tiny whitish particle on the surface image of the coated membrane which was suggested to have been as a result of silica (SiO_2) bonding on membrane surface.

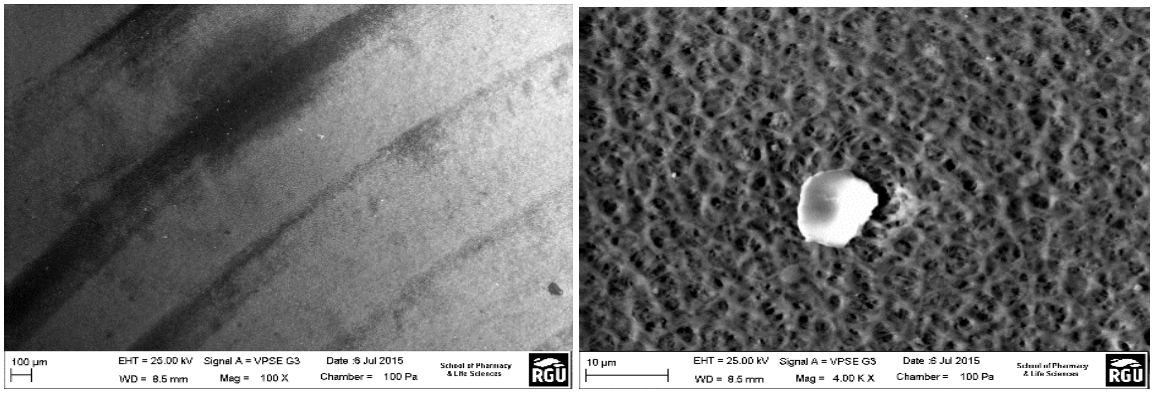

Fig 14a and b: SEM surface images of support (14a) and SEM surface image of silica membrane (14b).

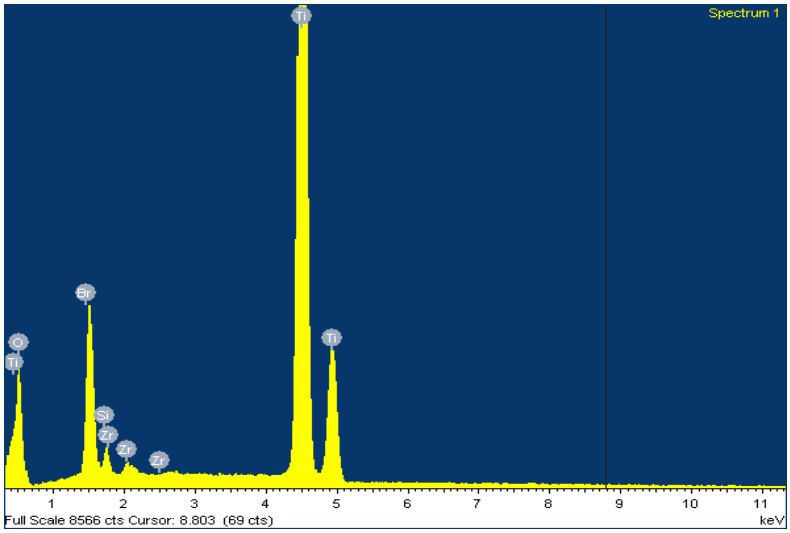

Figure 15: EDAX spectra of silica membrane.

4. Conclusion

The evaluation performance of a α-alumina nano-porous silica composite membrane for esterification applications was tested using Knudsen flow mechanism of transport. Four different gases were used for the analysis including Ar, He, N_2 and CO_2. The gas flux as a function of the gauge pressure was based on the respective molecular weight of the gases confirming Knudsen flow mechanism of transport. The FTIR-ATR of the silica membrane showed up to 5 bands on the spectra in contrast to that of the support with 3 bands on the spectra. He gas with the least molecular weight exhibited a higher flow rate with respect to the gauge pressure. The structural compounds on the FTIR of the membrane were identified to include C-H, O-H and C=C bonds. The surface area of the 8^{th} dip-coated silica membrane was found to be higher in contrast to the 7^{th} dip-coated membrane. After the 8^{th} modification process, the membrane pore size was found to reduce which confirms the effect of the silica membrane. The gas viscosity value with respect to the permeance exhibited a viscous flow mechanism of gas transport. The gas permeance was found to decrease with an increasing gauge pressure confirming limitation due to mass transfer. Helium gas was selected from the permeation test as the suitable carrier gas for the analysis of esterification products. The SEM of support showed a clear surface without evidence` of crack while SEM micrograph of the silica membrane exhibit a bonding on the surface of the membrane as result of the modification process. The EDAX elemental composition of the membrane showed the presence of SiO_2 compound. The support membrane exhibited a positive activation energy with N_2 gas in contrast to other gases while the silica membrane exhibited a negative activation energy with the gases. The mass spectra of the reaction product reflect the structure of ion number 45 confirming the presence of ethyl lactate compound using the NIST library spectra of GC-MS.

Other compounds including formic acid (71), 2,3-butandiol (73) and oxirane (75), were also detected on the spectra. The retention time of ester product was in the range of 2.128 – 7.756 minutes.

Acknowledgements

The Authors acknowledge the Centre for Process Integration and Membrane Technology (CPIMT) at RGU for providing the research infrastructure and the School of Pharmacy and Life science for the SEM image and FTIR analysis. Additionally, the sponsorship provided by the petroleum technology development fund (PTDF) is gratefully acknowledged.

Nomenclature

P = permeance (mol $m^{-2}s^{-1}Pa^{-1}$)

P_0 = Arrhenius-type pre–exponential constant (m^2s^{-1}),

T = temperature (K)

Ea = activation energy ($Jmol^{-1}$) of surface diffusion or heat of adsorption

R = gas molar constant (8.314621 $Jmol^{-1}K^{-1}$).

A = Surface area of the membrane (m_2)

L = length of the membrane (m),

r_1 = Membrane outer pore diameter (m),

r_2 = Membrane inner pore diameter (m),

π = constant (3.142).

J = Flux (mol s^{-1} m^{-2})

Q = Gas flow rate (mol s^{-1})

ΔP = Pressure drop across the membrane (bar).

References

[1] Li X, Liang B. Permeance of pure vapours in porous γ-Al2O3/α-Al2O3 ceramic membrane. *Journal of the Taiwan Institute of Chemical Engineers.* 2012; 43(3):339-346.

[2] Javaid A. Membranes for solubility-based gas separation applications. *Chemical Engineering Journal.* 2005; 112(1):219-226.

[3] Asthana NS, Kolah AK, Vu DT, Lira CT, Miller DJ. A kinetic model for the esterification of lactic acid and its oligomers. *Industrial & Engineering Chemistry Research.* 2006; 45(15):5251-5257.

[4] Fan Y, Zhou C, Zhu X. Selective catalysis of lactic acid to produce commodity chemicals. *Catalysis Reviews.* 2009; 51(3):293-324.

[5] Hasegawa S, Azuma M, Takahashi K. Stabilization of enzyme activity during the esterification of lactic acid in hydrophobic ethers and ketones as reaction media that are miscible with lactic acid despite their high hydrophobicity. *Enzyme and microbial technology.* 2008; 43(3):309-316.

[6] Aparicio S, Halajian S, Alcalde R, García B, Leal JM. Liquid structure of ethyl lactate, pure and water mixed, as seen by dielectric spectroscopy, solvatochromic and thermophysical studies. Chemical Physics Letters. 2008; 454(1):49-55.

[7] Aparicio S, Alcalde R. The green solvent ethyl lactate: an experimental and theoretical characterization. Green Chemistry. 2009; 11(1):65-78.

[8] Lomba L, Giner B, Zuriaga E, Gascón I, Lafuente C. Thermophysical properties of lactates. Thermochimica Acta. 2014; 575(0):305-312.

[9] Ugur Nigiz F, Durmaz Hilmioglu N. Green solvent synthesis from biomass based source by biocatalytic membrane reactor. International Journal of Energy Research. 2015; .

[10] Vu DT, Lira CT, Asthana NS, Kolah AK, Miller DJ. Vapor-liquid equilibria in the systems ethyl lactate ethanol and ethyl lactate water. Journal of Chemical & Engineering Data. 2006; 51(4):1220-1225.

[11] Tanaka K, Yoshikawa R, Ying C, Kita H, Okamoto K. Application of zeolite T membrane to vapor-permeation-aided esterification of lactic acid with ethanol. *Chemical Engineering Science.* 2002; 57(9):1577-1584.

[12] Li W, Liu W, Xing W, Xu N. Esterification of Acetic Acid and n-Propanol with Vapor Permeation Using NaA Zeolite Membrane. *Industrial & Engineering Chemistry Research.* 2013; 52(19):6336-6342.

[13] McCool BA, Hill N, DiCarlo J, DeSisto WJ. Synthesis and characterization of mesoporous silica membranes via dip-coating and hydrothermal deposition techniques. *Journal of Membrane Science.* 2003; 218(1–2):55-67.

[14] Lee D, Oyama ST. Gas permeation characteristics of a hydrogen selective supported silica membrane. *Journal of Membrane Science.* 2002; 210(2):291-306.

[15] Zhu J, Fan Y, Xu N. Modified dip-coating method for preparation of pinhole-free ceramic membranes. *Journal of Membrane Science.* 2011; 367(1):14-20.

[16] Smart S, Liu S, Serra JM, Diniz da Costa JC, Iulianelli A, Basile A. 8 - Porous ceramic membranes for membrane reactors. In: Basile A, editor. *Handbook of Membrane Reactors.* : Woodhead Publishing; 2013. p. 298-336.

[17] Barma S, Mandal B. Synthesis and characterization of ordered mesoporous silica membrane: Role of porous support and gas permeation study. *Microporous and Mesoporous Materials.* 2015; 210:10-19.

[18] Benito JM, Conesa A, Rubio F, Rodríguez MA. Preparation and characterization of tubular ceramic membranes for treatment of oil emulsions. *Journal of the European Ceramic Society.* 2005; 25(11):1895-1903.

[19] Lu G, da Costa JD, Duke M, Giessler S, Socolow R, Williams R, et al. Inorganic membranes for hydrogen production and purification: a critical review and perspective. *Journal of colloid and interface science.* 2007; 314(2):589-603.

[20] Mulder M. *Basic Principles of Membrane Technology Second Edition.* : Kluwer Academic Pub; 1996.

[21] Ismail AF, Khulbe KC, Matsuura T. *Gas Separation Membranes.* : Springer; 2015.

[22] Lee H, Yamauchi H, Suda H, Haraya K. Influence of adsorption on the gas permeation performances in the mesoporous alumina ceramic membrane. *Separation and Purification Technology.* 2006; 49(1):49-55.

[23] Weidenthaler C. Pitfalls in the characterization of nanoporous and nanosized materials. *Nanoscale.* 2011; 3(3):792-810.

[24] Kim, Hyung-Ju; Yang, Hee-Chul; Chung, Dong-Yong; Yang, In-Hwan; Choi, Yun Jung; Moon, Jei-kwon Functionalized Mesoporous Silica Membranes for CO2 Separation Applications. Journal of Chemistry, Hindawi Publishing Corporation, 2015, Article ID 202867, 9 pages.

[25] Xomeritakis G, Naik S, Braunbarth C, Cornelius CJ, Pardey R, Brinker C. Organic-templated silica membranes: I. Gas and vapor transport properties. *Journal of Membrane Science.* 2003; 215(1):225-233.

[26] Edward G. 2006. Apparatus and Method for separating gases. United state patent. Patent No.: US 7,048,778 B2. Robert Gordon University, Aberdeen, UK.

[27] Edidiong O, Habiba S, Kajama M, Edward G. An Experimental Study of Catalysts and Carrier Gas Transport through Membranes for Improved Yield of Ester Product. *Transactions on Engineering Technologies.* : Springer; 2016. p. 139-150.

[28] Zhang Y, Ma L, Yang J. Kinetics of esterification of lactic acid with ethanol catalyzed by cation-exchange resins. Reactive and Functional Polymers. 2004; 61(1):101-114.

[29] Okon E, S Habiba and Gobina E. Batch Process Esterification of Lactic acid catalysed by cation-exchange resins for the production of environmental-friendly solvent, Lecture Notes in Engineering and Computer Science: Proceedings of the World Congress on Engineering and Computer Science 2015, WCECS 2015, 21-23 October, 2015, San Francisco, USA, pp 623-628.

[30] Han HH, Ryu SH, Nakao S, Lee YT. Gas permeation properties and preparation of porous ceramic membrane by CVD method using siloxane compounds. *Journal of Membrane Science.* 2013; 431(0):72-78.

[31] Okon E, Shehu H, Gobina E. Gas Transport Through Inorganic Ceramic Membrane and Cation-Exchange Resins Characterization for Ethyl Lactate Separation. Transactions on Engineering Technologies: Springer; 2015. p. 403-414.

[32] Okon E, Shehu H, Gobina E. Novel Application of Gas Transport Properties with Ceramic Membrane for VOC Emission and Lactic Acid Esterification. *European Journal of Engineering and Technology Vol.* 2014; 2(2).

[33] Wall Y, Braun G, Brunner G. Gas transport through ceramic membranes under super-critical conditions. *Desalination.* 2010; 250(3):1056-1059.

[34] Araki S, Mohri N, Yoshimitsu Y, Miyake Y. Synthesis, characterization and gas permeation properties of a silica membrane prepared by high-pressure chemical vapour deposition. *Journal of Membrane Science.* 2007; 290(1):138-145.

[35] Lee H, Suda H, Haraya K. Gas permeation properties in a composite mesoporous alumina ceramic membrane. *Korean Journal of Chemical Engineering.* 2005; 22(5):721-728.

[36] Marković A, Stoltenberg D, Enke D, Schlünder E, Seidel-Morgenstern A. Gas permeation through porous glass membranes: Part I. Mesoporous glasses—effect of pore diameter and surface properties. *Journal of Membrane Science.* 2009; 336(1):17-31.